Current-voltage characteristics of quantum-point contacts in the closed-channel regime: Transforming the bias voltage into an energy scale

K. Gloos,[1,2] P. Utko,[1] M. Aagesen,[1] C. B. Sørensen,[1] J. Bindslev Hansen,[3] and P. E. Lindelof[1]
[1]*Nano-Science Center, Niels Bohr Institute fAFG, University of Copenhagen, Universitetsparken 5, DK-2100 Copenhagen, Denmark*
[2]*Wihuri Physical Laboratory, Department of Physics, University of Turku, FIN-20014 Turku, Finland*
[3]*Department of Physics, Technical University of Denmark, DK-2800 Lyngby, Denmark*
(Received 30 August 2005; revised manuscript received 2 November 2005; published 20 March 2006)

We investigate the $I(V)$ characteristics (current versus bias voltage) of side-gated quantum-point contacts, defined in GaAs/$Al_xGa_{1-x}As$ heterostructures. These point contacts are operated in the closed-channel regime, that is, at fixed gate voltages below zero-bias pinch-off for conductance. Our analysis is based on a single scaling factor, extracted from the experimental $I(V)$ characteristics. For both polarities, this scaling factor transforms the change of bias voltage into a change of electron energy. The latter is determined with respect to the top of the potential barrier of the contact. Such a built-in energy-voltage calibration allows us to distinguish between the different contributions to the electron transport across the pinched-off contact due to thermal activation or quantum tunneling. The first involves the height of the barrier, and the latter also its length. In the model that we are using the channel length remains the only adjustable parameter since the barrier height can be experimentally determined. For short ($\sim$0.06 μm) contacts, the $I(V)$-derived lengths agree rather well with those estimated from the geometrical layout, whereas nominally long ($\sim$1.2 μm) contacts are typically found to consist of very short ($\sim$0.2 μm) barriers. We have mapped the height of the barrier as a function of the gate voltage, and found that its behavior differs strongly from that extrapolated using conventional bias spectroscopy in the open-channel regime above conductance pinch-off.

DOI: 10.1103/PhysRevB.73.125326 PACS number(s): 73.23.−b, 73.63.Rt, 73.40.Gk, 85.30.Mn

I. INTRODUCTION

The conductance quantization across narrow constrictions, the so-called quantum-point contacts (QPCs), was discovered in 1988 by van Wees *et al.*[1] and Wharam *et al.*[2] Those constrictions, typically defined in a two-dimensional electron gas (2DEG), are so narrow relative to the Fermi wavelength of the 2DEG that the available energy levels of the one-dimensional (1D) subbands become well separated from each other. The main interest in the properties of QPCs has focused so far on the conductance quantization in the open-channel regime. However, a few applications exist where a QPC is operated in the closed-channel regime below zero-bias pinch-off for conductance. In such a case the sufficiently narrowed QPC channel forces the electron eigenenergies to emerge from the Fermi sea, thus suppressing electron flow at low bias voltages.

A closed QPC can be used, for example, as a source of hot electrons. One side of the constriction is then biased in such a way that its chemical potential is raised near the top of the point contact barrier. Hence, the electrons can tunnel (at low temperatures) to the other side of the point contact. Their excess energy is determined by the bias voltage. Those hot electrons can then be used to study the properties of a second, separate QPC in the closed regime,[3] or to control the number of electrons in a quantum dot as described, for example, in Ref. 4. In another application, a surface acoustic wave (SAW) is employed to drag electrons across the potential hill of a closed QPC. The resultant current is quantized in units of ef, the product of the electron charge e and the SAW frequency f.[5] Such devices could provide a new metrological current standard. No clear-cut model exists yet for the basic mechanism behind the SAW-induced single-electron transport.[6,7] Therefore, to understand this latter type of experiment it would be very useful to know not only the height of the QPC barrier, but also its shape or potential distribution. To find out how this barrier behaves in the closed-channel regime is the main topic of this paper.

The confinement potential of a QPC can be modeled by a realistic saddle-point approximation.[8] Here we use, however, a simpler scheme in which the QPC is represented by a hard-wall potential with eigenenergies[9]

$$E_n(w) = \frac{n^2h^2}{8m^*w^2} \tag{1}$$

where the QPC channel has a certain width $w(x)$. Here h is Planck's constant, $m^*=0.067m_e$ is the effective electron mass in GaAs, and the index n denotes the different one-dimensional energy subbands. Current flows in the x direction, whereas the gates of the QPC confine the electron wave functions in the y direction.

The width of the constriction may be approximated by an inverted Gaussian

$$w(x) = w_0\exp\left(\frac{x^2}{L^2}\right) \tag{2}$$

where w_0 is the minimum width of the unbiased constriction at a fixed gate voltage, and L defines its length. At the narrowest part of the constriction the subbands peak at $E_{n0}\approx 5.5$ eV $[n^2/w_0^2$ (nm)]. Although real QPCs are unlikely to reproduce exactly $w(x)$ as described by Eq. (2), this model can be easily analyzed. Since the width of the constriction can be adjusted using the gate voltage V_g, the length L of the

channel is the only parameter that characterizes the QPC and which has to be determined experimentally.

When w_0 increases, the consecutive 1D subbands lower their maximum energies and move below the Fermi level ϵ_F one after another. At low bias voltages $V \approx 0$ each subband n fully submerged in the Fermi sea carries a current proportional to V, contributing $G_n=(2G_0)\mathcal{T}_n$ to the total conductance G. Here, $\mathcal{T}_n$ is the transmission coefficient across the potential barrier of the nth subband. Thus, for ideal transmission $\mathcal{T}_n=1$ the conductance is quantized in units of twice the quantum conductance $G_0=e^2/h$. For QPCs with long channels the plateaus observed in the conductance may be systematically lower than the ideal multiples of $2e^2/h$. This is probably due to scattering processes inside the channels and due to an enhanced role of electron-electron interactions.[10–13]

The length of the potential barrier of a QPC can be estimated from how the conductance $G(V_g)$ and, more specifically, the steps between the conductance plateaus, change with energy or with temperature.[14] The only adjustable parameter is then the curvature of the potential barrier at its maximum defined by $\omega_x=2\sqrt{\epsilon_F/m^*}/L$ using Eqs. (1) and (2) as described below. In the following, the bottom of the conduction band on the drain side of the QPC is always considered as the reference (zero) point for the introduced energies. When the contact starts to open, the top of the barrier of the lowest subband E_{10} (at zero bias) is just slightly above the Fermi level, and the conductance varies like $G(E_{10}) \propto \exp[-2\pi(E_{10}-\epsilon_F)/\hbar\omega_x]$ at low temperatures.

The energy–gate voltage relation $E_{n0}(V_g)$ in the open-channel regime can be derived from bias-spectroscopy experiments where the conductance derivative dG/dV_g is probed with respect to both the gate voltage V_g and the bias voltage V, yielding the typical diamondlike transconductance pattern.[9,15,16] This assumes, however, that the potential energy around zero bias varies exactly like the applied bias voltage, that is it changes like $-eV$, with respect to the top of the barrier.

II. THE CLOSED-CHANNEL REGIME

The behavior of the $I(V)$ characteristics of QPCs in the closed regime, below zero-bias pinch-off for conductance, has received a lot of attention ever since the first experimental observation by Kouvenhowen *et al.*[17] A general introduction to the problem was later provided by Heinzel *et al.* in Ref. 18.

The bias voltage applied to the QPC changes the total barrier experienced by an electron. That is, at large biases the zero-bias limit, which is valid for spectroscopy in the open-channel regime, does not apply any more. The details of this change are unknown. In the classical description the bias voltage is assumed to drop across the QPC like[18,19]

$$dV \propto \frac{dx}{w(x)}. \tag{3}$$

When the width of the constriction varies like Eq. (2), the resulting additional electrostatic energy due to the bias voltage

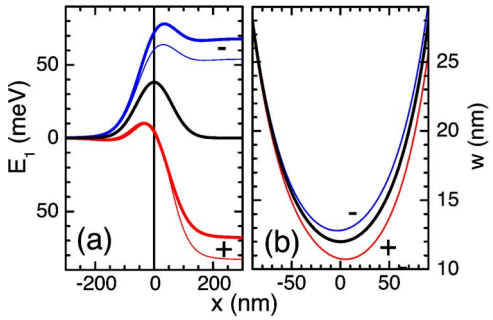

FIG. 1. (Color online) Schematic variation of (a) the potential barrier $E_1(x)$ as well as (b) the width $w(x)$ along the QPC channel. The following parameters were used: $w_0=12$ nm and $L=100$ nm. Thick solid lines describe the QPC at zero bias as reference and the biased QPC without self-gating. The negative (–) and positive (+) bias voltages were chosen to set the minimum barrier height at $E=\epsilon_F+\Delta E=10$ meV. The thin solid lines show the barrier height and width when the self-gating is included in the calculations. For this example, self-gating is assumed to change the channel width by 30 nm/V.

$$E_{bias} \approx -\frac{eV}{2}\left[1+\tanh\left(\frac{5x}{2L}\right)\right] \tag{4}$$

has to be added to the bare potential $E_n(x)$ of the nth subband given by Eq. (1). The bias voltage not only changes the maximum energy of the QPC potential barrier but also shifts the position of this maximum along the channel as illustrated in Fig. 1(a).

Using this model one can derive the current as function of bias voltage. At low currents and high bias voltages, only the first subband contributes,

$$I(V) = \frac{2e}{h}\int \mathcal{T}_1(\epsilon)\Delta f(\epsilon,V)d\epsilon, \tag{5}$$

where $\mathcal{T}_1(\epsilon)$ denotes the transmission probability for an electron of energy ϵ. The difference between the Fermi functions on both sides of the QPC $\Delta f(\epsilon,V)=f(\epsilon-\epsilon_F-eV)-f(\epsilon-\max[\epsilon_F,eV])$ ensures that electrons can only flow from occupied to empty states of the subband.

At high temperatures, thermal activation dominates the charge transport through the point contact. Therefore only the height of the barrier matters. The probability for thermal activation is then described by the Boltzmann factor $\exp[(\epsilon-E_{max})/(k_BT)]$ where $E_{max}(V)$ is the maximum of the total potential of the first subband. This results in the (1D) Richardson's law

$$I(E) = \frac{e\sqrt{\pi}}{h}k_BT\exp\left(-\frac{E}{k_BT}\right) \tag{6}$$

with $E=E_{max}-\epsilon_F$ for positive biasing. For negative biasing the current reverses its sign, and $E=E_{max}-\epsilon_F+eV$.

In the low-temperature limit quantum tunneling dominates. Unlike thermal activation, it depends not only on the height of the barrier but also on its shape. We approximate the potential hill of the QPC by an inverted parabola with the curvature $d^2E_1(x)/dx^2=-m^*\omega_x^2$ of the total potential. This

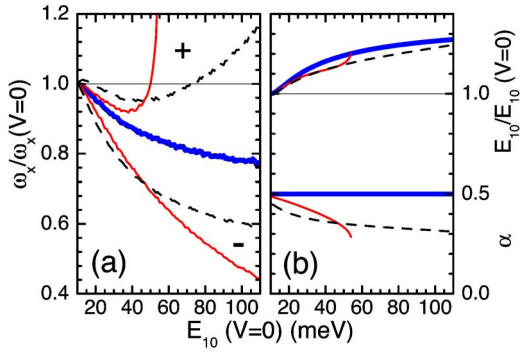

FIG. 2. (Color online) Calculated curvature parameter ω_x, barrier height E_{10}, as well as the α parameter as function of the gate-voltage-dependent barrier height $E_{10}(V=0)$ of the unbiased QPC. The negative (–) and the positive (+) bias voltage were chosen to set the minimum barrier height at $E=10$ mV, as in Fig. 1. (a) Curvature parameter ω_x normalized with respect to its zero-bias value. Without self-gating, the results for negative and positive polarity coincide (thick solid line), while they differ when self-gating is included (thin solid lines). (b) Barrier height E_{10} normalized to the height at zero bias as well as the α parameter. Without self-gating (thick solid lines) and with self-gating (thin solid lines). These parameters have been derived as follows. For each barrier height at zero bias $E_{10}(V=0)$ the critical voltages $V_{+/-}$ are first determined as for the point contact in Fig. 1. Then the curvature parameters are calculated from the total potentials, and E_{10} as well as α from $V_{+/-}$ as described in the text. When the effect of self-gating is included (assumed here to change the channel width by 30 nm/V as in Fig. 1), the curvature parameter for positive polarity diverges above about 55 meV, and both E_{10} and α cannot be determined for higher barriers. The dashed lines in (a) and (b) were obtained when a weakened self-gating at large barriers was assumed, according to Fig. 14 below.

simplification is justified because only electron states near the top of the barrier contribute to the tunneling current, while those far below are effectively blocked.[18] Figure 2(a) shows that the curvature, represented by the parameter ω_x, varies only weakly with applied bias voltage. Therefore we can write, independently of bias voltage,

$$\omega_x(V) \approx \omega_x(0) = \frac{2}{L}\sqrt{\frac{E_{10}(0)}{m^*}}. \tag{7}$$

In the Wentzel-Kramers-Brillouin (WKB) approximation the transmission coefficient through a parabolic barrier is given by[8]

$$\mathcal{T}_1(\epsilon) = \left[1 + \exp\left(-\frac{2\pi(\epsilon - E_{max})}{\hbar\omega_x}\right)\right]^{-1}. \tag{8}$$

Thus at low temperatures Eq. (5) becomes

$$I(E) \approx \frac{e\omega_x}{2\pi^2}\exp\left(-\frac{2\pi E}{\hbar\omega_x}\right). \tag{9}$$

This reproduces the similar exponential dependence found for the zero-bias conductance close to the pinch-off, and delivers directly the length L of the QPC. However, an energy–bias voltage calibration is required to compare the theoretical $I(E)$ curves with the experimental $I(V)$ data. The energy scale assumed for the bias-spectroscopy experiments in the open-channel regime does not apply to the closed-channel regime as becomes obvious, for example, from the strongly asymmetric $I(V)$ characteristics in the latter limit.

The calibration in the closed-channel regime can be achieved as follows.[20] A positive bias applied to the source contact of the QPC lowers both the chemical potential $\mu_s = \epsilon_F - eV$ on the source side of the point contact and the top of the potential barrier. Our central assumption, which is supported by the experimental results presented below, is that the height of the barrier changes proportionally to the bias voltage. At the threshold bias V_+, the top of the barrier is lowered to the unshifted chemical potential $\mu_d = \epsilon_F$ on the drain side, kept at virtual ground. Thus, electrons can flow from drain to source. Figure 1(a) illustrates how the barrier changes with bias voltage. For positive biasing, we describe the necessary reduction of the barrier height by

$$\frac{E_{10} - \epsilon_F - \Delta E}{e} = \alpha V_+. \tag{10}$$

Here, ΔE is a small energy offset that depends on the current at which V_+ is read off, and α describes the asymmetry of the $I(V)$ characteristics. On the other hand, a negative bias voltage raises the chemical potential on the source side as well as the top of the barrier. At the critical voltage

$$V_- = -\frac{E_{10} - \epsilon_F - \Delta E}{e} + \alpha V_- \tag{11}$$

the chemical potential μ_s reaches the barrier within ΔE and electrons start to flow from source to drain. Combining Eqs. (10) and (11) yields

$$\alpha = \frac{V_-}{V_- - V_+}. \tag{12}$$

Without self-gating $\alpha = 0.5$, as confirmed by the model calculations in Fig. 2(b).

The height of the barrier with respect to the highest one of the chemical potentials is reduced by $\delta E = e\alpha V$ for positive and $\delta E = e(\alpha - 1)V$ for negative bias voltages, respectively. For both polarities this transforms the change of the bias voltage into an energy scale, independent of ϵ_F and the yet unknown (though small) ΔE. Hence, *each* $I(V)$ characteristic contains its own energy-voltage calibration.

The $I(V)$ characteristics of the closed QPC can now be used to *measure* the absolute height of the barrier at zero bias using

$$E_{10}(V=0) \approx E_{10} = e\alpha V_+ + \epsilon_F + \Delta E. \tag{13}$$

The only assumption made here is that for both polarities the barrier height changes in the same manner. The small energy difference ΔE depends on the current threshold at which the critical voltages $V_{+/-}$ are read off, as discussed above. Applying this procedure is justified by the model that we use. Figure 2 shows that without self-gating the curvature calculated at $V_{+/-}$ is only slightly smaller than the zero-bias value, while the barrier height derived from $V_{+/-}$ is slightly larger than the height at zero bias. Those deviations are a direct result of the

asymmetry introduced by the bias voltage. They are enhanced when the barrier height increases, that is, when larger bias voltages have to be applied to enforce a current flow. However, at those large barriers the deviations seem to saturate at around 20–30% off their respective zero-bias values. Thus the underestimate of ω_x is partly compensated by the overestimated energy scale.

Self-gating due to the bias voltage affects the shape of the QPC channel. In the configuration discussed here, the gate voltage is always applied with respect to the drain contact. At zero bias, the voltage difference between the channel and the gates is constant along the constriction. This is no longer true when the bias voltage is applied to the source contact. Then only the drain side of the QPC channel is kept at zero potential, while the bias voltage drops continuously across the constriction, as described approximately by Eq. (4). Thus the effective gate voltage, that is the difference between the voltage applied to the gates V_g and the local voltage in the QPC channel $V(x)=-E_{bias}(x)/e$, changes along the constriction. This introduces an asymmetry of the channel width. To the first order, the width changes then by

$$\delta w = \beta \delta(V_g - V(x)), \tag{14}$$

with a proportionality constant[21] $\beta=2\times 4\epsilon\epsilon_0/\pi e n_{2D}$ that depends on the relative dielectric constant ϵ and the sheet density n_{2D} of the 2DEG. Typical experimental data yield as order of magnitude $\beta\approx 0.1$ μm/V, as determined from the bias-spectroscopy experiments on side-gated samples as in Ref. 22. Figure 1 shows schematically how self-gating changes the potential barrier as well as the width of the QPC channel: A positive (negative) bias voltage lowers (raises) the maximum of the total potential and shifts its position towards the drain (source) contact of the QPC. On the other hand, including self-gating itself increases (decreases) the barrier height while its maximum is shifted toward the source (drain). Thus both mechanisms counteract each other.

When self-gating is included, the curvature parameter differs for the two polarities. For negative biasing ω_x becomes smaller, while for positive biasing it becomes larger than without self-gating. And the asymmetry parameter α can be strongly reduced by including self-gating, as indicated in Fig. 2. This is because for sufficiently high barriers, such large positive bias voltages may be required to drive a current through the QPC that can completely close the contact. This indicates possible limits of the reliability of our analysis.

We have investigated shallow-etched QPCs with a potential barrier supposedly varying smoothly on a length scale of $0.1-1$ μm. It has turned out that our geometrically long point contacts comprise instead one (or more) very short ($L\approx 0.2$ μm) barriers. Our analysis is based on the nonlinear $I(V)$ characteristics in the closed-channel regime. Each $I(V)$ curve is modeled by a scaling factor α that transforms the change of the bias voltage into a change of the electron energy with respect to the top of the QPC barrier, as discussed above. This, in turn, allows us to distinguish between thermally activated transport over the barrier and quantum tunneling through the barrier. The latter directly involves the length of the barrier as the only adjustable parameter.

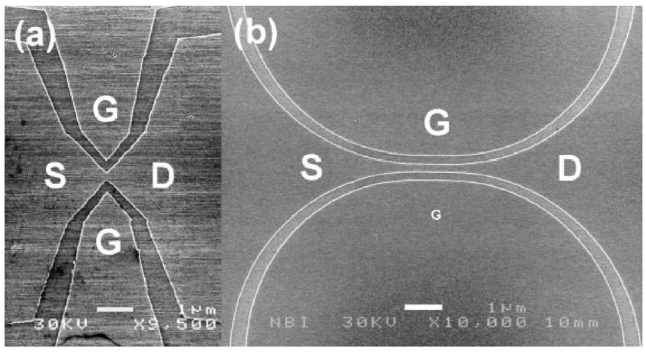

FIG. 3. Scanning-electron micrograph of (a) the short and (b) the long QPC. The white horizontal bars define a length of 1 μm. The bright thin lines mark the trench edges where material has been etched away to deplete the 2DEG below. The bias voltage V is applied to the source contact (S), and the current I is measured at the drain contact (D). Electrodes on top and bottom serve as side gates (G).

III. EXPERIMENTAL DETAILS

The quantum point contacts fabricated for the purposes of this study were patterned on GaAs/Al_xGa_{1-x}As heterostructures using electron-beam lithography. Each QPC was defined by two shallow-etched trenches which formed a narrow constriction between two electron reservoirs, whereas the 2DEG regions on both sides of the channel served as the side gates.[22,23] Two different types of QPCs were investigated, either with as short a channel as possible or with a long constriction. The two different layouts are shown in Figs. 3(a) and 3(b), respectively.

For QPCs with a short barrier, two trenches were shaped as sharp tips facing each other, as in Fig. 3(a). They were defined on a heterostructure wafer with a 2DEG mobility of 70 m^2/V s and a carrier density of $n_{2D}=1.9\times 10^{15}$ m^{-2}, both measured in the dark at 10 K. This corresponds to $\epsilon_F\approx 7$ meV and an electron mean free path of approximately 5 μm. On the other hand, the long QPCs were defined by two 200 nm wide and 40 nm deep semi-circular trenches with a curvature radius of 5 μm and a 1 μm long straight segment in its center. The scanning-electron micrograph in Fig. 3(b) shows that this long channel varies uniformly and very smoothly. The 2DEG had a mobility of 54 m^2/V s and carrier density $n_{2D}=3\times 10^{15}$ m^{-2}. The corresponding Fermi energy was $\epsilon_F\approx 11$ meV and the electron mean free path of the 2DEG was approximately 5 μm.

Figure 4 shows schematically how the width changes along the channel of the short and the long QPC, respectively. For this figure we took into account the contours of the shallow-etched trenches in the micrographs of Fig. 3. Those contours were vertically shifted to obtain an arbitrary chosen minimum width of 10 nm. The potential distribution along the center of the QPC was then calculated using the hard-wall potential Eq. (1). For this we assumed that the minimum width, like any other width, can be adjusted by the gate voltage without affecting the shape of the channel. According to those figures the length of the QPC barrier is $L\approx 0.06$ and 1.2 μm for the short and the long QPC, respectively.

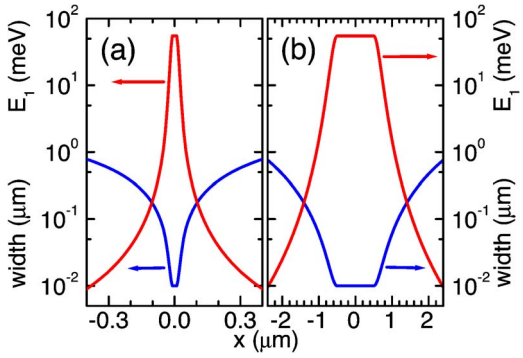

FIG. 4. (Color online) Schematic width and potential distribution for the first subband E_1 along the channel of (a) the short and (b) the long QPC. For both samples a minimum width of 10 nm was assumed.

All measurements described in the following were carried out in the vacuum can of a ^{3}He refrigerator with a base temperature of 0.3 K. We describe here in detail results obtained for two samples: one short QPC (sample number HCO-194-030303-1-4) and one long QPC (SAW 6A). Similar results were also obtained for other devices, with either short or long channels.

For both types of point contacts quantized steps in the conductance characteristics $G(V_g)$ could be observed at $T=4.2$ K (Fig. 5). However, at lower temperatures the long QPC had pronounced conductance fluctuations that were almost absent for the short QPC. After taking into account the $\sim 600\ \Omega$ series resistance of the contact pads and the 2DEG, the conductance plateaus of the long QPC were found to be roughly 40% below the ideal multiples of $2G_0=2e^2/h$.[20] For the short QPC the plateaus appeared, however, almost at the ideal multiples of $2G_0$. We discuss this difference in the next section.

In at least one case the low-temperature conductance fluctuations of the long QPC developed into Coulomb-blockade peaks at low temperatures, as shown in Fig. 6. Such current oscillations appeared at regular intervals along the V_g axis,

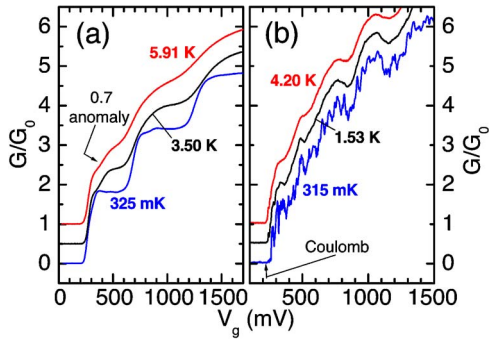

FIG. 5. (Color online) Typical normalized conductance G/G_0 versus gate voltage V_g at the indicated temperatures for (a) a short and (b) a long QPC. The curves are displaced vertically in steps of 0.5. These are the raw data, that is the $\sim 600\ \Omega$ serial resistances of the contact pads and 2DEG are not subtracted. The so-called 0.7 anomaly of the short QPC as well as the position of the Coulomb-blockade anomaly of the long QPC are marked.

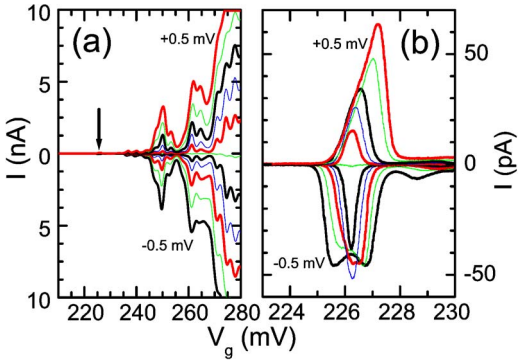

FIG. 6. (Color online) (a) Current I versus gate voltage V_g of the long QPC at $T=315$ mK [see Fig. 5(b)]. The point contact was biased from $V=-0.5$ to $+0.5$ mV in steps of 0.1 mV. The arrow marks the position of the Coulomb blockade anomaly, shown in detail in (b).

close to the pinch-off voltage for conductance. Their bias dependence in Fig. 6(b) resembled those reported, for example, in Ref. 24.

Figure 7 shows that the width as well as the height of the Coulomb-blockade peak in the zero-bias conductance varied with temperature, without saturating at the base temperature of $T=0.3$ K. This demonstrates that external electrical noise was negligible. Clear conductance fluctuations as well as Coulomb-blockade peaks already indicate a *structured* QPC, which in fact consists of two (or more) separate barriers instead of a single one.

When the point contacts were operated in the open-channel regime, bias-spectroscopy experiments yielded $dV/dV_g \approx 0.01$ for both the long and the short QPC. Characteristic energies $\hbar\omega_x \approx 1$ meV were estimated from the temperature dependence of the conductance in a similar way as in Ref. 14. More accurate estimates were not possible because of the 0.7 anomaly of the short QPC and the strong conductance fluctuations of the long QPC, respectively.

IV. THE ASYMMETRY PARAMETER OF THE $I(V)$ CHARACTERISTICS

Figure 8 shows typical $I(V)$ characteristics obtained for both devices at fixed gate voltages below the conductance

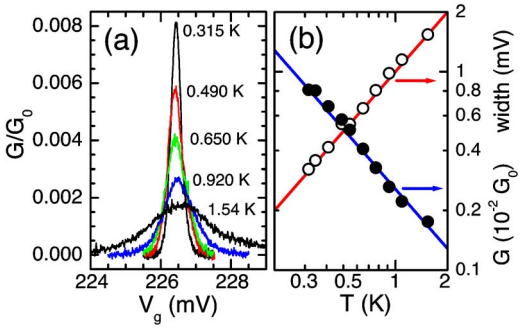

FIG. 7. (Color online) Coulomb-blockade anomaly of the long QPC. (a) Normalized zero-bias conductance G/G_0 versus gate voltage V_g at the indicated temperatures. (b) Width (open symbols) and height (closed symbols) of the Coulomb peak versus temperature. The solid lines vary as T and $1/T$, respectively. There is no saturation at the lowest temperature.

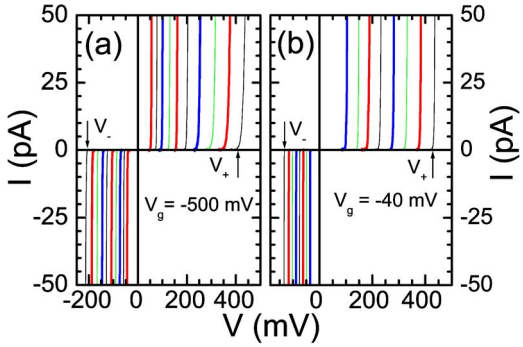

FIG. 8. (Color online) Typical characteristics of current I versus bias voltage V. (a) The short QPC at $T=3.3$ K and at gate voltages from −500 to −50 mV in steps of 50 mV. (b) The long QPC at 0.3 K and gate voltages from −40 to 100 mV in steps of 20 mV. Arrows mark V_- and V_+ for the indicated gate voltages.

pinch-off that is in the closed-channel regime. They resemble those already demonstrated in Ref. 17: No current flows around zero bias, but there is an abrupt onset of current at $V=V_-$ and $V=V_+$ when the critical bias voltages are reached. In our experiments, the magnitude of V_+ was always larger than V_-, while the slope of the current at positive polarity was always smaller than that at negative polarity. This agrees well with the results obtained by others.[17]

We have chosen to read off $V_{+/-}$ at a small current of 1 pA, still well above the detection limit. At those conditions the chemical potential on one side of the QPC must be raised to within ΔE, that is a few meV, below the top of the barrier to enable charge transport by either thermal activation or quantum tunneling. We have found that the experimentally determined asymmetry parameters $\alpha=V_-/(V_--V_+)$ are rather insensitive with respect to the current at which $V_{+/-}$ are read off as well as to the temperature.

Despite the huge bias voltages applied to the point contacts, heating due to hot-electron effects should be negligible since in the investigated current-voltage range Joule heating is only ~0.1 pW or less. In the worst case, that is for positive biasing of the source contact, one of the electron reservoirs may be heated to 50 mK above the 0.3 K base temperature of the refrigerator (and much less than that at higher temperatures). In Ref. 20 we describe how to estimate this increase of the 2DEG temperature due to hot electrons. Even this little heating does not matter here because for both polarities the reservoir, from which the electrons start their travel through the QPC, remains cold. It is the temperature of this reservoir that determines the probability for thermal activation and the broadening of the Fermi distribution of the conduction electrons.

Figure 9 shows the magnitude of the measured current as function of $\delta E=e\alpha V$ and $\delta E=e(\alpha-1)V$ for positive and negative polarity of the bias voltages, respectively. Both the short as well as the long QPC behave in a very similar manner.

(a) The originally asymmetric $I(V)$ characteristics transform into current-energy characteristics $I(\delta E)$ that are nearly straight lines in a semilogarithmic plot. The $I(\delta E)$ traces obtained for negative and positive polarity almost coincide with

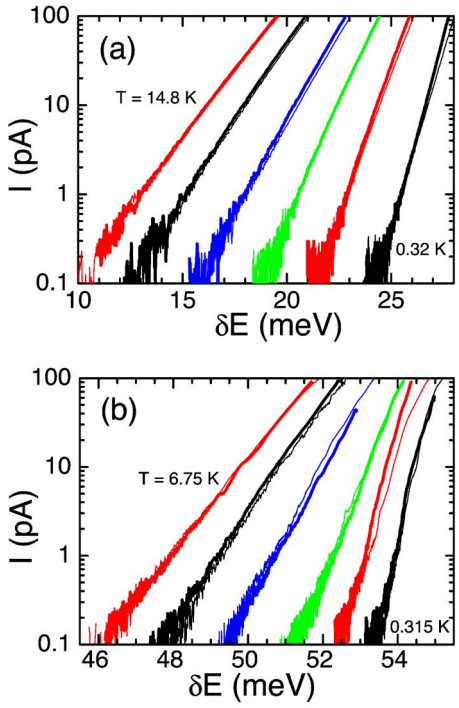

FIG. 9. (Color online) Magnitude of the current I versus change of energy δE. (a) The short QPC at $T=14.8, 12.9, 10.4, 8.4, 5.5$, and 0.32 K (from left to right). The asymmetry parameter was $\alpha=0.33$, and the gate voltage was fixed at $V_g=-100$ mV. (b) The long QPC at $T=6.75, 5.94, 4.57, 3.15, 1.82$, and 0.315 K (from left to right). For this contact $\alpha=0.235$ and $V_g=100$ mV. For both contacts traces for positive (thick) and negative (thin solid lines) polarity are almost identical.

each other, indicating their proper scaling using the experimentally determined parameter α.

(b) At low temperatures the slope of $I(\delta E)$ (in a semilogarithmic plot) is not sensitive to the temperature at which the measurement is carried out. But at higher temperatures, it decreases strongly with increasing T. The slope of $I(\delta E)$ can be described in terms of an effective temperature T_{eff} using the relation for thermal activation $I \propto \exp(\delta E/k_B T_{eff})$. (Note that δE measures how much the barrier is reduced.) The dependencies of T_{eff} on the temperature of the sample are shown in Fig. 10 for the short and long QPC, respectively. Since the slope of $I(\delta E)$ does not depend on T at low temperatures, the corresponding T_{eff} saturates in this regime. We attribute this saturation to the crossover from thermally activated transport at high T to quantum tunneling at low T. The latter should be expected as the dominant process for the short QPCs. But for the long point contact, tunneling should be negligible almost down to our base temperature of 0.3 K.

(c) Figure 10 shows that at high T the effective temperature determined for the short QPC approaches the asymptote as $T_{eff} \approx \sqrt{T^2+T_0^2}$ with $T_0 \approx 6$ K. The long QPC follows a similar relation, though with a smaller $T_0 \approx 2.5$ K. Note that the latter asymptote is enhanced by $T_{eff} \approx 1.4T$. Figure 2 shows that the energy scale could be overestimated by about 20%. The remaining difference between T_{eff} and the measured T that is observed at high temperature could then be due to an additional voltage drop inside the long channel of

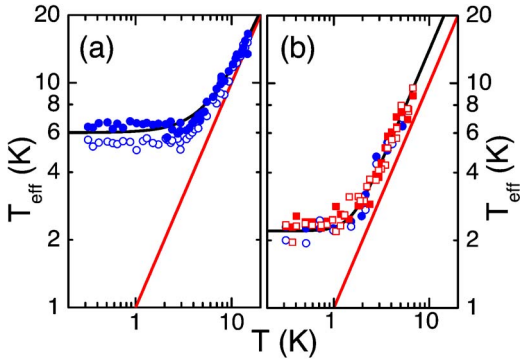

FIG. 10. (Color online) Effective temperature T_{eff} versus temperature T of (a) the short QPC and (b) the long QPC (two different colours for two series of measurements). Open and solid symbols represent results for negative and positive polarities, respectively. Solid lines are guides to the eye with $T_{eff}=\sqrt{T^2+(6\ \mathrm{K})^2}$ and $T_{eff}=\sqrt{(1.4T)^2+(2.5\ \mathrm{K})^2}$, respectively. The offset by a factor of 1.4 is discussed in the text. The straight solid lines indicate $T_{eff}=T$.

the QPC, leading to a further overestimate of δE. Such a parasitic voltage drop would also explain why the plateaus of the quantized conductance in Fig. 5(b) are far below the ideal multiples of $2G_0$. If that was the case, the real T_0 of this sample would be about 2.1 K.

(d) At low temperatures the slopes of the $I(\delta E)$ traces in a semilogarithmic plot, and therefore T_{eff}, may differ for the two polarities of the applied bias voltages. See Fig. 10(a), where these differences are small, and also Fig. 15 below, where the differences are large. In most cases we have found that T_{eff} is larger for positive than for negative polarity. This could be explained by tunneling for which, unlike for thermal activation, both the height and the length of the barrier matter. And because of self-gating, the effective tunneling length depends on polarity, resulting in a shorter (longer) barrier at positive (negative) bias voltages.

(e) Figure 11 shows that the effective temperature T_{eff} is rather robust with respect to changes of the gate voltage, as

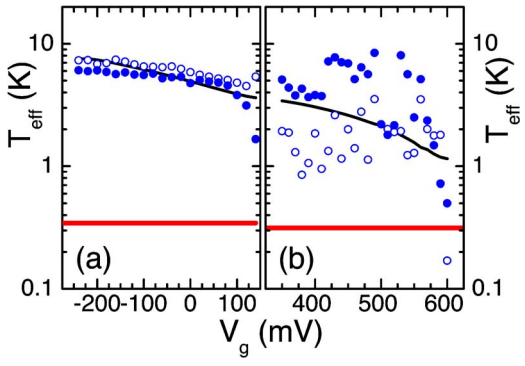

FIG. 11. (Color online) Effective temperature T_{eff} versus gate voltage V_g of (a) the short and (b) the long QPC. Thick solid lines indicate the sample temperature slightly above $T=0.3$ K. Open and solid symbols represent results for negative and positive polarities, respectively. Zero-bias conductance pinch-off is at about 100 and 650 mV for (a) and (b), respectively. The thin lines through the data points show how $T_0=T_{eff}$ should vary if the dependence of E_{10} on V_g is taken into account.

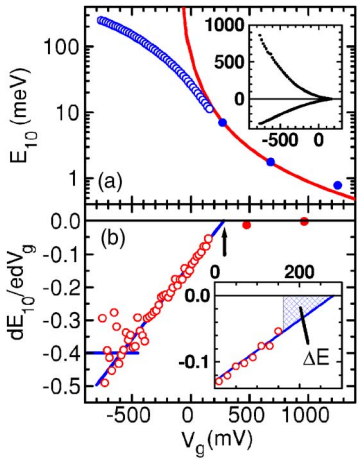

FIG. 12. (Color online) (a) Barrier height E_{10} of the short QPC versus gate voltage V_g. The $\Delta E\approx 4$ meV offset as well as the Fermi energy $\epsilon_F=7$ meV have been taken into account while determining the height in the closed-channel regime (open symbols). Estimated barrier heights in the open-channel regime are included as well (closed symbols). The solid line shows how the barrier height would change if the hard-wall potential and a linear variation of the depletion width with gate voltage was assumed. The inset shows the original V_+ (top) and V_- (bottom) data versus gate voltage in mV units. (b) Derivative of $E_{10}(V_g)$ from (a). The transition to the first conductance plateau has its center at around 220 mV, indicated by the arrow. The solid lines fit tentatively the linear as well as the constant part. The inset shows in detail how to estimate the offset ΔE.

long as the QPC remains in the closed-channel regime. The short QPC seems to reveal a trend for higher T_0 at lower gate voltages. This could be partly attributed to the weak dependence of ω_x on the barrier height in Eq. (7). On the other hand, the energy scale can be overestimated by about 20%, while at the same time the zero-bias curvature is underestimated by a similar amount. Figure 2(a) shows that ω_x is larger for positive than for negative polarity. This corresponds to observing larger T_{eff} for positive biasing than for negative one. For both types of samples the average supplied power (at 1 pA) changes by a factor of 10, from ~100 to ~10 fW when the gate voltage is increased from its lowest to its largest value. The absence of a corresponding increase of T_{eff} at low gate voltages confirms that heating effects are negligible.

V. MAPPING THE BARRIER HEIGHT

To drive a current through a QPC operated far below the zero-bias conductance pinch-off, large bias voltages have to be applied. This usually leads to leakage, that is a parasitic and uncontrollable current flows from the source or the drain to the gates. Leakage may also lead to a rearrangement of impurities near the QPC channel that can change irreversibly the overall characteristics of the sample or even destroy it. In only few cases of our experiments the applied bias voltage range could be as large as in Figs. 12 and 13.

For a given gate voltage below the conductance pinch-off, the height of the QPC barrier at zero bias E_{10} can be deter-

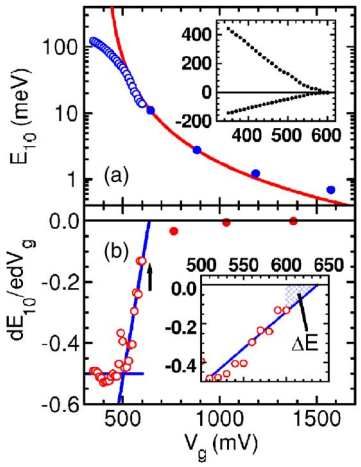

FIG. 13. (Color online) (a) Barrier height E_{10} of the long QPC versus gate voltage V_g. The $\Delta E \approx 2.7$ meV offset as well as the Fermi energy $\epsilon_F = 11$ meV have been taken into account while determining the height in the closed-channel regime (open symbols). Estimated barrier heights in the open-channel regime are included (closed symbols). The solid line shows how the barrier height would change if the hard-wall potential and a linear variation of the depletion width with gate voltage was assumed. The inset shows the original V_+ (top) and V_- (bottom) data versus gate voltage in mV units. (b) Derivative of $E_{10}(V_g)$ from (a). The transition to the first conductance plateau has its center at around 640 mV, indicated by the arrow. The two solid lines are guides to the eye. The inset shows in detail how to estimate the offset ΔE.

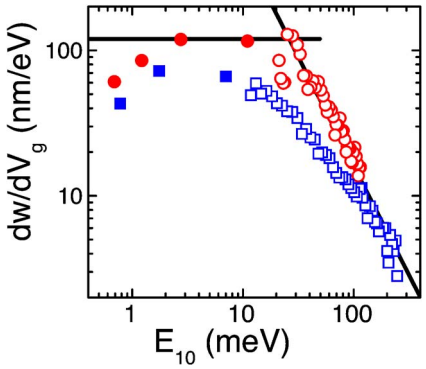

FIG. 14. (Color online) The depletion width per gate voltage dw/dV_g versus barrier height E_{10}. Squares and circles are for the short and the long QPC, respectively. Open symbols are the data in the closed-channel regime; closed symbols are estimates from the position of the conductance steps of the open-channel contacts. In the ideal case one would expect a constant dw/dV_g, while at large barrier heights the data follow $dw/dV_g \propto E^{-3/2}$ as indicated by the solid lines for the long QPC.

mined from the $I(V)$ characteristic taken at this specific value of V_g, as already described in Sec. II. Figure 12(a) shows the change in the barrier height that occurs for the short QPC in response to the gate voltage. The resulting $E_{10}(V_g)$ trace, estimated using Eq. (13), deviates strongly from the data extrapolated from the open-channel regime. The numerical derivative of the barrier height dE_{10}/dV_g is plotted in Fig. 12(b). At low gate voltages ($V_g < -500$ mV), the derivative appears to saturate at around $dE_{10}/dV_g \approx -0.4e$. On incrementing the gate voltage above $V_g \approx -500$ mV, the magnitude of dE_{10}/dV_g decreases in a roughly linear manner. At large gate voltages, the derivative must approach zero asymptotically as dictated by the results of bias spectroscopy in the open-channel regime. Thus there seem to be two, maybe three, different regimes for the evolution of the barrier height, depending on whether the contact is open or closed. Figure 13 shows a similar analysis for the long QPC.

Additional information can be obtained from the area enclosed by the extrapolated derivative and the V_g axis. This area, indicated by the shaded region in the insets to Figs. 12(b) and 13(b), describes the energy difference ΔE between Fermi level and top of the barrier. When the current of just $I = 1$ pA is used to read off the critical voltages $V_{+,-}$, we estimate $\Delta E \approx 4.0$ and 2.7 meV for the short and the long QPC, respectively.

The floating energy scales in Fig. 9 can also be fixed by applying Eq. (9) for the tunnel current and using $T_0 = \hbar \omega_x / 2\pi k_B$ in the tunneling regime by comparing with Eq. (6). The short QPC has $\omega_x \approx 5.2 \times 10^{12}$ s^{-1}, while the long one has $\omega_x \approx 2.2 \times 10^{12}$ s^{-1}. At a certain current, say $I = 1$ pA, the energy difference between the Fermi level and the top of the barrier is then $\Delta E \approx 5.5$ and 2.1 meV, respectively. Both values fit well the estimates in Figs. 12 and 13.

In the open-channel regime, a continuous observation of the barrier height is not possible. For the short QPC, the transitions to the first three conductance plateaus occur at around $V_g = 270$, 680, and 1250 mV [see Fig. 5(a)]. At these transitions the height of the first, the second, and the third 1D subband, respectively, coincides with ϵ_F. According to Eq. (1), at those transitions the height of the first subband should thus be $E_{10} = \epsilon_F$, $\epsilon_F/4$, and $\epsilon_F/9$. Correspondingly, the average derivatives are around $-0.025e$ and $-0.005e$ at around $V_g = 370$ and 670 mV.

Our experiments thus show that, assuming the hard-wall potential, the depletion width of the 2DEG varies linearly with gate voltage only for wide channels, that is, in the open-channel regime. When the contact is closed at low gate voltages, the barrier height increases less strongly than extrapolated from the open-contact regime. A natural explanation for this deviation, a kind of saturation, might be that the barrier height can not exceed the conductance band edge of the GaAs/Al$_x$Ga$_{1-x}$As heterostructure of around 0.3 eV.

Applying our basic Eq. (1) for the hard-wall potential, the depletion width changes like

$$\frac{dw}{dV_g} = -\frac{1}{2}\sqrt{\frac{h^2}{8m^* E_{10}^3}}\frac{dE_{10}}{dV_g}. \tag{15}$$

The resulting data are plotted in Fig. 14 using the $E_{10}(V_g)$ characteristics of Figs. 12 and 13. The derivative of the channel width dw/dV_g remains constant at low barriers in the open-channel regime, but drops strongly for barriers larger than about 10 meV. Since this transition appears near the Fermi energy one might suspect that it is just the conducting-insulating transition of the QPC which is responsible for the strong reduction of the depletion width. On the other hand we cannot exclude that the hard-wall potential fails for very narrow channels and large barriers.

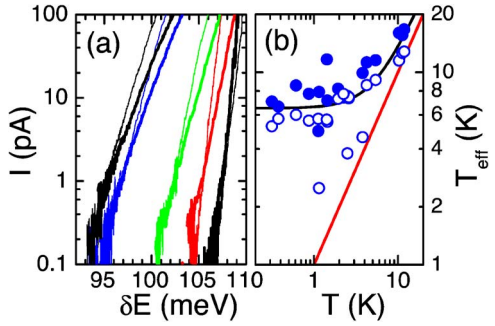

FIG. 15. (Color online) (a) Magnitude of the current I versus change of energy δE of the long QPC for a second stable configuration. Temperatures are $T=10.3, 11.9, 5.43, 3.80$, and 0.315 K (from left to right). Thin (thick) solid lines represent negative (positive) polarity. (b) Effective temperature T_{eff} versus temperature T. Open (closed) symbols denote negative (positive) polarity. The solid line is a guide to the eye with $T_{eff}=\sqrt{(1.2T)^2+(6.5\ \mathrm{K})^2}$. The offset at high temperatures is discussed in the text. The straight line is $T_{eff}=T$.

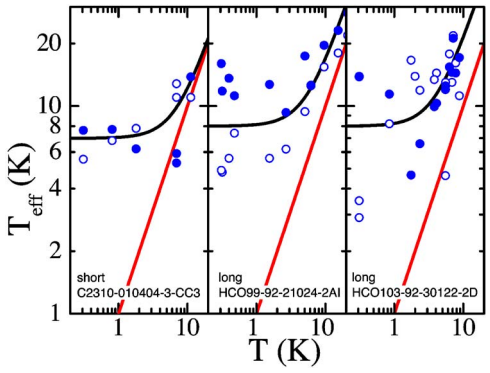

FIG. 16. (Color online) Effective temperature T_{eff} versus temperature T of one short and two long QPCs. Open and closed symbols denote negative and positive polarity, respectively. The straight solid lines are $T_{eff}=T$. The lines through the data points discussed in the text are guides to the eye.

VI. LENGTH OF THE QUANTUM-POINT CONTACTS

Since the exact shape of the potential barrier is unknown, we use Eq. (9) for a qualitative analysis. A straightforward estimate gives

$$L \approx \sqrt{\frac{E_{10}}{m^*}}\frac{\hbar}{\pi k_B T_0} \approx 118\ (\mathrm{nm}) \times \frac{\sqrt{\mathrm{E_{10}\ (meV)}}}{T_0\ (\mathrm{K})} \qquad (16)$$

for the length of the QPC. Note that the systematic deviations, shown in Fig. 2, between the curvature parameter ω_x of the biased and unbiased point contacts are almost compensated by overestimating the energy scale.

The short QPC in Fig. 9(a) has a $T_0 \approx 6$ K and a barrier height $E_{10}=\delta E(1\ \mathrm{pA})+\epsilon_F+\Delta E(1\ \mathrm{pA}) \approx 37$ meV at zero bias. Thus its length is $L \approx 0.12\ \mu$m, which agrees reasonably with the expected length. The long QPC in Fig. 9(b) has a $T_0 \approx 2.5$ K and a barrier height $E_{10} \approx 67$ meV at zero bias. This yields the length of $L \approx 0.38\ \mu$m, much shorter than expected from the geometrical layout.

Thermal cycling of the long QPC gave different stable configurations. A switching between different stable states occasionally occurred as well during the same cool down. Figure 15 shows T_{eff} for such a case where the pinch-off voltage for zero-bias conductance was increased from $V_g \approx 0.25$ to 0.65 V and the saturated T_0 from 2.5 to 6.5 K (and at $E_{10} \approx 115$ meV). Because of the higher T_0 the length $L \approx 0.19\ \mu$m of this barrier would be much shorter than the dominant barrier calculated from Fig. 10(b). The strong scatter of data points in Fig. 15(b) for the two different polarities at low temperatures again points to quantum-tunneling effects or the results of the large E_{10}. Here T_{eff} are again larger for positive than for negative polarities, as expected from Fig. 2(a).

We have investigated the temperature dependence of three other samples in less detail, one short and two long QPCs. Their layout, Fermi energy, and electronic mean free path were similar to those for the short and the long QPC that were described before. The data for the three additional devices are summarized in Fig. 16. The short QPC (C2310-010404-3-CC3) had a $T_0 \approx 7$ K, whereas the two long ones had $T_0 \approx 8$ K. However, at high temperatures in the thermal regime, one of the long QPCs (sample HCO103-92-30122-2D) had very large T_{eff}. This coincided with a strongly reduced height of the conductance plateaus in the open-channel regime of this device. Therefore it is true that T_0 should be downscaled accordingly to about $T_0 \approx 4$ K. For the other long QPC, sample HCO99-92-21024-2AI, this offset of T_{eff} at high temperatures was much smaller.

In addition, we have investigated several other long QPCs at a fixed low temperature (1.7 K). These samples also had effective temperatures of order $T_{eff} \approx 10$ K, indicating short potential barriers.

Surprisingly a short barrier determines the main properties of all our long QPCs. Such a short barrier could be caused by a single impurity sitting in the channel. The occurrence of different stable states could then result from different impurities being the dominating one, and hence representing a changed environment. Those impurities could be the randomly distributed Si donors in the GaAlAs doping layer of the heterostructure. Depleting the 2DEG in the closed-contact regime means that those donors are no longer screened as for an open contact. They should then have a spatial extension of around 50 nm,[25,26] which compares well to the experimentally determined barrier length of our nominally long QPCs. Such impurities do not move around easily. But the bias voltage shifts the position of maximum of the potential barrier along the channel. This continuous motion is superposed on the static potential of the unbiased contact. The latter could consist of several peaks of comparable size instead of a single one. By changing the bias voltage the dominant potential peak could be switched, possibly resulting in the large scattering of data points in Figs. 15(b) and 16.

A more interesting—but highly speculative—alternative would be that the constriction forms spontaneously, possibly triggered by a nearby impurity. This would be analogous to the recently discussed spontaneous formation of a single-spin state in a QPC to explain the 0.7 conduction anomaly.[27]

VII. CRITICAL ESTIMATE OF THE ACCURACY OF OUR RESULTS

Our analysis of the experimental data is based on many simplifying assumptions, which are introduced in order to restrict the number of adjustable parameters. For example, we could have used a softer potential to model the QPC constriction, instead of the hard-wall potential. This would have required, however, at least one additional free parameter that could not be fixed from the available data. We believe that our simplifying approach, with a minimum set of adjustable parameters, is justified by the results, especially by the successful transformation of the $I(V)$ characteristics for both polarities into single $I(\delta E)$ curves, as shown in Fig. 9.

The absolute error in determining T_{eff} is less than 10% in the best case, where the QPC has a single well-defined barrier [see Fig. 11(a)]. The accuracy of the T_{eff} readout can be, however, further deteriorated if the QPC consists of two or more barriers, as seems to be the case in Fig. 11(b). When the bias voltage is changed, the QPC might, for example, switch from one dominant barrier to another one.

We note that the presence of one (or more) additional barrier(s) in our nominally long constrictions was in one case clearly confirmed by Coulomb blockade peaks below conductance pinch-off, as shown in Figs. 6 and 7. However, such peaks were not observed at all cooldowns even of the same sample. For the Coulomb oscillations to appear, a quantum dot has to be accidentally formed in the constriction. This strongly depends on the specific spatial configuration of the impurities, and requires two barriers of comparable height. On the other hand, the analysis performed using our model is not limited by such a condition, and in principle allows us to probe the length of the dominant potential barrier of the QPC.

Heating of the 2DEG due to external high-frequency noise could easily saturate T_{eff} at low temperatures. However, the temperature dependence of the Coulomb peaks observed for one of our devices (Fig. 7) confirms that the 2DEG, and even the electron system in the quantum dot itself, was at the same temperature as measured by the thermometer. Hence, heating effects can be safely excluded.

In Sec. II, we already pointed out that the barrier height (and thus the energy scale) can be overestimated by up to about 20% above its zero-bias value (see Fig. 2). However, possible systematic errors due to this effect are partly compensated when the length of the barrier is determined. We estimate that the lengths derived from the data in Figs. 9 and 10, and based on the model Eq. (2), are underestimated by about 10%. This systematic deviation increases for stronger self-gating, which is indicated by the splitting up of $I(\delta E)$ for the two polarities.

The absolute value of the barrier length is not well established. This length depends strongly on how it is defined and what functional behavior $w(x)$ is assumed along the QPC channel. Our measurements yield information only about the curvature ω_x at the top of the barrier, provided that this top approaches the chemical potential of one side of the QPC. The parts of the barrier well above or well below that chemical potential are not accessible in those kinds of experiments. This is because electrons in such energy ranges have either vanishingly small or very large transmission coefficients, as discussed in detail in Ref. 18. Thus, the absolute value of the length is not very relevant, only its size relative to that of another QPC. In our analysis, we have compared two different types of QPCs with each other, using the same model for the potential barrier. We have also compared the experimental data with the $w(x)$ dependence estimated from the geometrical layouts of each of the constrictions, like those shown in Fig. 4. Both methods yielded the same result, namely, that our nominally long QPCs actually consist of rather short barriers, with lengths comparable to those determined for the short QPCs.

VIII. CONCLUSIONS

We have presented a simple, straightforward method to extract the energy–bias voltage calibration from the asymmetric $I(V)$ characteristics of a QPC in the closed-channel regime when the zero-bias conductance is pinched off. By analyzing those contacts, we could distinguish between thermally activated and tunneling transport across the QPC.

As a second application we have mapped the barrier height of the QPCs in the closed-channel regime as function of gate voltage. We observed strong deviations from the expected behavior that could be caused by the finite conduction-band edge of the $GaAs/Al_xGa_{1-x}As$ heterostructures as the natural limit for the barrier height.

Our main result, however, is that the length of the QPC barrier can be derived from such simple $I(V)$ characteristics at low temperatures. This length is the only parameter that can be adjusted in the model that we are using, since both the barrier height and its curvature are experimentally accessible. Surprisingly, the properties of our long QPCs are determined by intrinsic ultrashort barriers.

As one practical consequence of our investigation we suggest reconsidering the general view of single-electron transport through allegedly long QPCs by a surface acoustic wave.[5,20,23] For those applications the QPC potential should vary smoothly on a length larger than the SAW wavelength. The SAW superposed on such a static potential barrier is then assumed to form moving quantum dots, carrying an integer number of electrons in each of its local minima. For our long QPCs this picture has to be revised since the dominant barrier seems to be an order of magnitude *shorter* than the typical ~ 1 μm SAW wavelength. Current quantization (or its absence for some of the SAW samples) in units of the elementary charge times the SAW frequency should be strongly affected by an *ultrashort* barrier. Recently, Fletcher *et al.*[28] reported on SAW experiments in which such a scenario might have been realized.

ACKNOWLEDGMENTS

We thank I. Farrer and D. A. Ritchie for supplying us with a wafer (C2310) used to fabricate one of our QPCs. This work was supported by the European Commission FET Project SAWPHOTON.

[1] B. J. van Wees, H. van Houten, C. W. J. Beenakker, J. G. Williamson, L. P. Kouwenhoven, D. van der Marel, and C. T. Foxon, Phys. Rev. Lett. **60**, 848 (1988).
[2] D. A. Wharam, T. J. Thornton, R. Newbury, M. Pepper, H. Ahmed, J. E. F. Frost, D. G. Hasko, D. C. Peacock, D. A. Ritchie, and G. A. C. Jones, J. Phys. C **21**, L209 (1988).
[3] A. S. Dzurak, C. J. B. Ford, M. J. Kelly, M. Pepper, J. E. F. Frost, D. A. Ritchie, G. A. C. Jones, H. Ahmed, and D. G. Hasko, Phys. Rev. B **45**, 6309 (1992).
[4] J. M. Elzerman, R. Hanson, L. H. Willems van Beveren, B. Witkamp, L. M. K. Vandersypen, and L. P. Kouwenhoven, Nature (London) **430**, 431 (2004).
[5] J. M. Shilton, V. I. Talyanskii, M. Pepper, D. A. Ritchie, J. E. F. Frost, C. J. B. Ford, C. G. Smith, and G. A. C. Jones, J. Phys.: Condens. Matter **8**, L531 (1996).
[6] K. Flensberg, Q. Niu, and M. Pustilnik, Phys. Rev. B **60**, R16291 (1999).
[7] A. M. Robinson and C. H. W. Barnes, Phys. Rev. B **63**, 165418 (2001).
[8] M. Büttiker, Phys. Rev. B **41**, R7906 (1990).
[9] L. I. Glazman and A. V. Khaetskii, Europhys. Lett. **9**, 263 (1989).
[10] L. Worschech, F. Beuscher, and A. Forchel, Appl. Phys. Lett. **75**, 578 (1999).
[11] S. J. Koester, B. Brar, C. R. Bolognesi, E. J. Caine, A. Patlach, E. L. Hu, H. Kroemer, and M. J. Rooks, Phys. Rev. B **53**, 13063 (1996).
[12] S. Tarucha, T. Honda, and T. Saku, Solid State Commun. **94**, 413 (1995).
[13] A. Yacoby, H. L. Stormer, N. S. Wingreen, L. N. Pfeiffer, K. W. Baldwin, and K. W. West, Phys. Rev. Lett. **77**, 4612 (1996).
[14] V. Senz, T. Heinzel, T. Ihn, S. Lindemann, R. Held, K. Ensslin, W. Wegscheider, and M. Bichler, J. Phys.: Condens. Matter **13**, 3831 (2001).
[15] N. K. Patel, J. T. Nicholls, L. Martin-Moreno, M. Pepper, J. E. F. Frost, D. A. Ritchie, and G. A. C. Jones, Phys. Rev. B **44**, 13549 (1991).
[16] K. J. Thomas, M. Y. Simmons, J. T. Nicholls, D. R. Mace, M. Pepper, and D. A. Ritchie, Appl. Phys. Lett. **67**, 109 (1995).
[17] L. P. Kouwenhoven, B. J. van Wees, C. J. P. M. Harmans, J. G. Williamson, H. van Houten, C. W. J. Beenakker, C. T. Foxon, and J. J. Harris, Phys. Rev. B **39**, 8040 (1989).
[18] T. Heinzel, D. A. Wharam, F. M. de Aguiar, J. P. Kotthaus, G. Böhm, W. Klein, G. Tränkle, and G. Weimann, Semicond. Sci. Technol. **9**, 1220 (1994).
[19] S. Ulreich and W. Zwerger, Superlattices Microstruct. **23**, 719 (1998).
[20] K. Gloos, P. Utko, J. Bindslev Hansen, and P. E. Lindelof, Phys. Rev. B **70**, 235345 (2004).
[21] L. I. Glazman and I. A. Larkin, Semicond. Sci. Technol. **6**, 32 (1991).
[22] A. Kristensen, H. Bruus, A. E. Hansen, J. B. Jensen, P. E. Lindelof, C. J. Marckmann, J. Nygård, C. B. Sørensen, F. Beuscher, A. Forchel, and M. Michel, Phys. Rev. B **62**, 10950 (2000).
[23] P. Utko, K. Gloos, J. Bindslev Hansen, and P. E. Lindelof, Acta Phys. Pol. A **103**, 533 (2003).
[24] E. B. Foxman, P. L. McEuen, U. Meirav, N. S. Wingreen, Y. Meir, P. A. Belk, N. R. Belk, M. A. Kastner, and S. J. Wind, Phys. Rev. B **47**, 10020 (1993).
[25] J. A. Nixon and J. H. Davies, Phys. Rev. B **41**, R7929 (1990).
[26] J. A. Nixon, J. H. Davies, and H. U. Baranger, Phys. Rev. B **43**, 12638 (1991).
[27] S. M. Cronenwett, H. J. Lynch, D. Goldhaber-Gordon, L. P. Kouwenhoven, C. M. Marcus, K. Hirose, N. S. Wingreen, and V. Umansky, Phys. Rev. Lett. **88**, 226805 (2002).
[28] N. E. Fletcher, J. Ebbecke, T. J. B. M. Janssen, F. J. Ahlers, M. Pepper, H. E. Beere, and D. A. Ritchie, Phys. Rev. B **68**, 245310 (2003).